Available online at www.sciencedirect.com
SCIENCE DIRECT®
Planetary and Space Science 53 (2005) 3–17
Planetary and Space Science
www.elsevier.com/locate/pss

A statistical study of the properties of interplanetary coronal mass ejections from 0.3 to 5.4 AU

Y. Liu*, J.D. Richardson, J.W. Belcher

Center for Space Research, Massachusetts Institute of Technology, MIT 37-655, Cambridge, MA 02139, USA

Accepted 12 September 2004

Abstract

We make a comprehensive survey of interplanetary coronal mass ejections (ICMEs) observed by the Helios 1 and 2, Ulysses, WIND and ACE spacecraft, which together cover heliocentric distances from 0.3 to 5.4 AU. The signatures used to identify ICMEs are enhanced helium abundances and depressed proton temperatures. We use the ICME list to study the radial evolution of ICMEs in a statistical sense. We find that ICMEs expand during propagation in the solar wind; the radial width increases as $R^{0.92}$. Most ICMEs (10 out of 13) observed at Ulysses from 5.15 to 5.4 AU seem to be co-moving with the solar wind. The density and magnetic field magnitude decrease faster with distance than the ambient solar wind, as expected for an expanding feature. The temperature, in contrast, decreases more slowly inside ICMEs than in the ambient solar wind, so the plasma in the ICMEs must be heated. The expansion behaves more like an isothermal than adiabatic process, with a polytropic index of $\gamma \sim 1.15$. This index is constant over distance and solar cycle, and is unchanged when the electron pressure and the magnetic pressure are included. The polytropic index for ICME electrons is less than unity ($\gamma_e \sim 0.73$), inconsistent with their decreasing temperature observed by Ulysses. The occurrence rate of ICMEs at 1 AU approximately tracks the sunspot numbers and the CMEs observed by LASCO, with a temporary reduction between 1998 and 1999. The radial width of near-Earth ICMEs has a solar cycle dependence, with a mean radial width of 0.34 AU.

Keywords: Solar wind; ICMEs; Propagation

1. Introduction

Coronal mass ejections (CMEs) are explosive processes of energy release in the solar atmosphere which can lead to significant expulsion of mass from the Sun. The ejected material in the solar wind, called interplanetary coronal mass ejections (ICMEs), is sometimes associated with shock waves and large southward interplanetary magnetic fields (IMFs) and can cause large geomagnetic disturbances. Southward IMF can induce magnetic reconnection at the dayside of the magnetopause (Dungey, 1961), which allows solar particles to enter the magnetosphere and drives substorm activity. Therefore, ICME investigation and forecasting are of great importance.

CMEs have been studied by remote sensing of these events at the Sun and by in situ measurements of their plasma properties when they encounter spacecraft. However, their global morphology and some basic processes involved with their propagation in the interplanetary space are not well understood. Two possible ICME structures are discussed in the literature. The first describes ICMEs as flux ropes which remain magnetically connected to the Sun while they are carried outward by the solar wind (e.g., Burlaga, 1988; Chen, 1996; Kumar and Rust, 1996; Bothmer and Schwenn, 1998). This scenario is supported by Kahler and Reames (1991), who showed evidence of a flare particle onset inside an interplanetary magnetic cloud (MC); MCs

*Corresponding author.
E-mail address: liuxying@space.mit.edu (Y. Liu).

0032-0633/$ - see front matter © 2004 Elsevier Ltd. All rights reserved.
doi:10.1016/j.pss.2004.09.023

constitute a subset of ICMEs. The other possibility is that ICMEs may be disconnected from the Sun and form spheromaks or plasmoids (Vandas et al., 1993a, b).

The propagation of ICMEs is also an outstanding problem. Based on ideal MHD solutions, Osherovich et al. (1993a, b) developed a self-similar model for the expansion of MCs that have a flux-tube geometry. This model requires a polytropic index of $\gamma < 1$ to allow the flux rope to expand, which is not supported by numerical simulations (e.g., Vandas and Fischer, 1996). Kumar and Rust (1996) proposed a toroidal flux-rope model for interplanetary MCs in which the dynamics and energetics of the propagation are governed by the conservation of magnetic helicity. In this model, the interaction of MCs with the ambient solar wind is neglected. Taking into account the drag force due to the surrounding medium, Chen (1996) advanced an alternative treatment of the mechanism for the propagation of common ICMEs. The theoretical and numerical approaches described above revealed important properties associated with ICMEs. However, some secondary processes and properties, such as ionic composition, the thermodynamic structure and formation of regions of southward IMF, are not well understood.

Observations of plasma features over a range of radial distances provide a way to quantitatively test and constrain models of transient structure evolution in the solar wind. One way to study the evolution of ICMEs is to track specific ICMEs through the heliosphere (Paularena et al., 2001; Richardson et al., 2002). This approach has the drawback that spacecraft at different heliospheric distances are rarely radially aligned. In this paper we use a statistical approach; we first make a comprehensive survey of ICMEs in the heliosphere from 0.3 to 5.4 AU using data from multiple spacecraft. We then use this survey to produce a statistical representation of ICME properties as a function of radial distance. Comparison of physical properties of ICMEs observed by different spacecraft explicitly assumes that an average over many ICMEs can represent the attributes of a typical event.

2. Multi-spacecraft observations

We use plasma and magnetic field data from Helios 1 and 2, WIND, ACE and Ulysses to search for ICMEs. Detailed descriptions of the instruments on these spacecraft can be found in the literature: for Helios mission, see Rosenbauer et al. (1981), Schwenn et al. (1975) and Musmann et al. (1975); for WIND, see Ogilvie et al. (1995) and Lepping et al. (1995); for ACE see Stone et al. (1998) and for Ulysses see Wenzel et al. (1989). Fig. 1 displays the heliocentric distance, heliolatitude and heliolongitude versus observing time for each spacecraft. The data from Helios 1 and 2 cover heliocentric distances from 0.3 to 1 AU and span the time interval from December 1974 through 1985. WIND and ACE have provided measurements of near-Earth solar wind conditions since 1994 and 1998, respectively. The observations of these four spacecraft are generally within $\pm 10^\circ$ of the ecliptic. Ulysses was launched in 1991 and explores the solar wind conditions at distances from 1 to 5.4 AU and up to 80° heliolatitude.

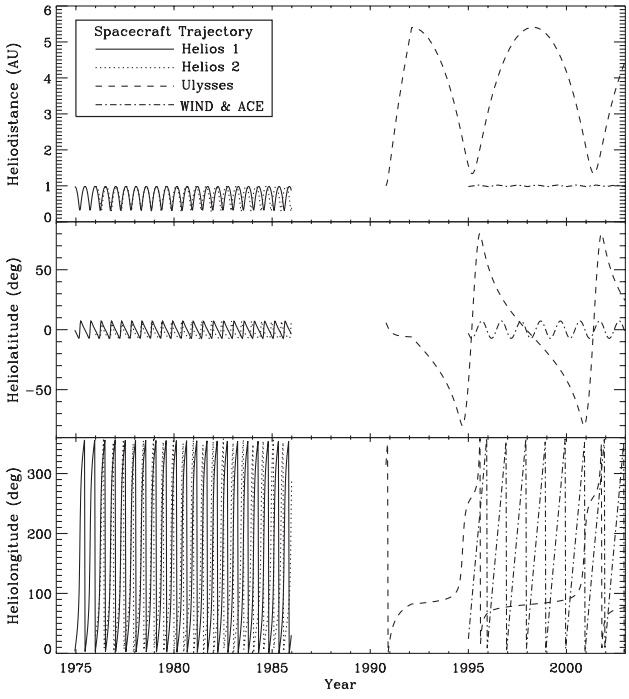

Fig. 1. Spacecraft heliocentric distance (upper panel), heliolatitude (middle panel) and heliolongitude (lower panel) as a function of time for the observations.

3. Data reduction and analysis

3.1. Criteria for picking ICMEs

Signatures of ICMEs identified in interplanetary space include depressed ion and/or electron temperatures (e.g., Gosling et al., 1973; Montgomery et al., 1974), enhanced helium abundance (Hirshberg et al., 1972; Borrini et al., 1982), bidirectional streaming of suprathermal electrons (e.g., Montgomery et al., 1974; Temnyi and Vaisberg, 1979; Gosling et al., 1987), bidirectional energetic ion flows (e.g., Rao et al., 1967; Palmer et al., 1978; Richardson and Reames, 1993), and smooth and strong magnetic fields (e.g., Burlaga et al., 1981; Gosling et al., 1987). One important subset of ICMEs, whose outstanding feature is smooth rotation of the magnetic field vector through a large angle, are

defined as MCs by Burlaga et al. (1981). We include all types of ICMEs in this study.

Despite these many ICME signatures, no universal standard can be used to identify ICMEs. Individual ICMEs rarely show all the signatures described above and no single distinctive feature is detected in all ICMEs (Richardson and Cane, 1993). Therefore, the identification of ICMEs remains a subjective undertaking. We use two criteria to pick the ICMEs in this study. The first is proton temperatures which are low for the observed solar wind speed, a condition generally present in ICMEs and which may be sufficient to identify ejecta (Richardson and Cane, 1995). The second is the alpha-to-proton density ratio, which rarely exceeds ~ 0.08 except in an ICME (Goldstein et al., 1998). The advantage of using the alpha-to-proton density ratio as an identifier is that it will not change as ICMEs evolve.

We first find all the times when the average alpha-to-proton density ratio $N_\alpha/N_p \geqslant 0.08$ or when the proton temperatures are low according to the criterion developed by Richardson and Cane (1995). This criterion uses the ratio $\frac{T_p}{T_{exp}}$, where T_p and T_{exp} are the observed temperature of protons and the expected temperature for solar wind plasma with speed v. If this ratio is $\leqslant 0.5$ the plasma is usually an ICME. The expected temperature T_{exp} (in units of 10^3 K) is calculated from the relationship obtained by Lopez and Freeman (1986) between the temperature and the speed for typical solar wind:

$$T_{exp} = \begin{cases} (0.0106v - 0.278)^3/R, & v < 500\ \mathrm{km\,s^{-1}}, \\ (0.77v - 265)/R, & v \geqslant 500\ \mathrm{km\,s^{-1}}. \end{cases} \quad (1)$$

To apply this relationship at various radial distances, we assume an R^{-1} temperature dependence (Totten et al., 1995). The macroscale T–v relation does not change appreciably with solar activity levels and is reproducible from diverse spacecraft plasma data (Burlaga and Ogilvie, 1973; Lopez and Freeman, 1986). In addition, this relationship is not affected by dynamic interplanetary processes and thus stays fixed at all distances and latitudes (Burlaga and Ogilvie, 1970, 1973; Richardson and Smith, 2003). Although the distance dependence of T_p may deviate from R^{-1} over large radial distances (Gazis et al. (1994) found $T \sim R^{-0.7}$ for data out to 10 AU and Richardson et al. (1995) found $T \sim R^{-0.5}$ using data out to 40 AU), we assume that the R^{-1} dependence holds for the 0.3–5.4 AU interval.

The low-temperature and high-helium abundance regions are not usually coincident. The occurrences of high helium abundance are often patchy, whereas the depressed proton temperature regions are usually more persistent. We combine these observations to determine the ICME boundaries. When data gaps are present, the ICME boundaries are inferred from the signatures which are available. Fig. 2 shows an example of an ICME identified by our criteria. This event was observed by Helios 1 at 0.61 AU on Day 121 of 1980. The density and temperature ratios corresponding to our ICME identification criteria are shown by dotted lines in the upper two panels. The alpha abundance in this ICME is greatly enhanced with a peak value exceeding 0.25. The two signatures exhibit good time coincidence, so the boundaries of this event are easily determined. Also shown is the bulk speed of the solar wind, which decreases nearly monotonically across the event, with a total speed decrease of about 30 km s^{-1}. The speed difference between the leading and trailing edges suggests that the ICME will radially expand as it moves outward. The duration of this event is about 14 h, which combined with the average speed of 300 km s^{-1} gives a radial width of 0.1 AU. The dotted line in the lowest panel is a linear fit to the time profile of the speed, which is used to estimate the expansion speed, $\Delta v = v_l - v_t$, where v_l and v_t are the speeds of the leading edge and the trailing edge of the ICME, respectively.

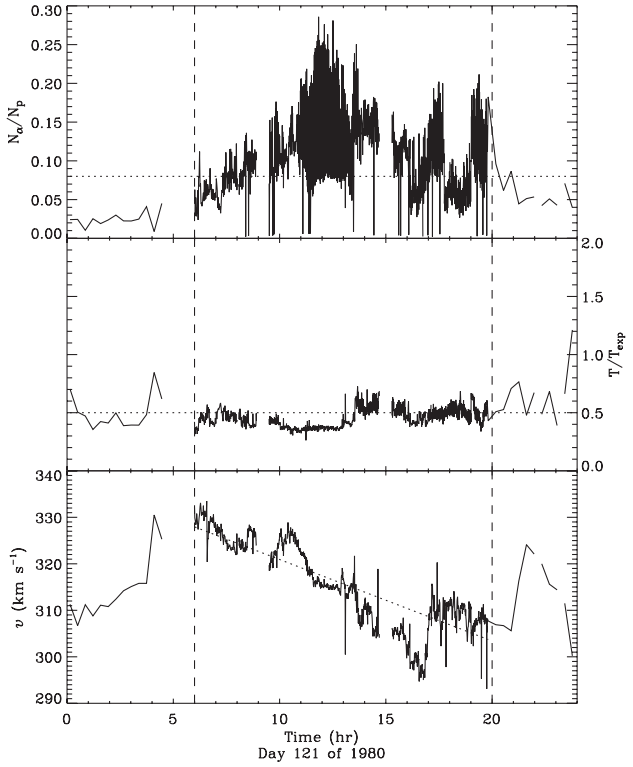

Fig. 2. An ICME (bracketed by the dashed lines) observed by Helios 1 at 0.61 AU on Day 121 of 1980. Shown from top to bottom are the alpha-to-proton density ratio, the observed-to-expected temperature ratio, and the bulk speed of the solar wind. The dotted lines in the upper two panels mark the threshold levels (lower bound for alpha-to-proton density ratio, upper bound for the observed-to-expected temperature ratio). The dotted line in the lowest panel is a linear fit to the speed profile which is used to get the expansion speed.

3.2. The list

Probable ICMEs are determined from the observations by applying the criteria described above. Since no universally accepted criteria are available to define an ICME, this list of events may not coincide with those identified by other researchers. Different ejecta may merge into a conglomeration that appears to be a single event, or an individual event may split into multiple ejecta. In such cases it is difficult to separate individual ICMEs. Fortunately these situations do not occur frequently, as shown by Cane and Richardson (2003).

Table 1 lists the ICMEs identified in the data sets using our criteria. The first column indicates the spacecraft used to identify the ICME and the second shows the year in which the ICME occurred. Events are not listed separately for WIND and ACE, since WIND and ACE both monitor the solar wind conditions near Earth and hence generally observe the same events. Events observed by one of those spacecraft but not the other are discarded. Before 1998, all 1 AU events are from the WIND data set. The third column denotes the start time of each ICME; the fourth column shows the duration of each ICME in hours. The different accuracies in the duration reflect the different time resolutions of the data sets for each spacecraft. The next three columns, which give the location of the spacecraft in the heliographic inertial frame, are the heliocentric distance, heliolongitude and heliolatitude. The next column shows the average speed for every ICME. As illustrated in Fig. 2, the bulk speed of a typical ICME decreases across the event; the average speed represents the motion of the ejecta as a whole. The second to last column shows the radial size of each event, which is the product of the average speed and the ICME duration. The last column indicates whether the event has been reported as an MC or an ICME in the Helios MC list (Bothmer and Schwenn, 1998), the Ulysses ICME list (http://swoops.lanl.gov/cme_list.html), the WIND MC list (http://lepmfi.gsfc.nasa.gov/mfi/mag_cloud_pub1.html) or the ACE MC list (http://www.bartol.udel.edu/~chuck/ace/ACElists/obs_list.html). Since our identification criteria are different from those of the lists mentioned above, even when events appear in both lists the time boundaries may not be the same.

We know of no other list of generic ICMEs based on the Helios observations. Therefore, our list for Helios 1 and 2 could be a resource for the study of ICME evolution in the inner heliosphere. For comparison, we indicated where our list overlapped the MC list of Bothmer and Schwenn (1998).

Examining our Ulysses ICME list shows that almost all the ICMEs are concentrated at low heliographic latitudes; no ICMEs were identified at Ulysses in 1994, 1995 or 1997. As reported by Phillips et al. (1995), high-latitude ICMEs may not have helium abundance enhancements, which is one of the signatures we use to identify ICMEs. In 1994 and 1995, the decreasing phase of solar cycle 22, Ulysses was above the solar south and north poles respectively (refer to Fig. 1). No events were identified in this time period, consistent with the on-line Ulysses ICME list. However, the absence of ICMEs on our list in 1997 cannot be explained in the same fashion; the ICMEs observed by Ulysses in this year did not meet our ICME criteria.

Cane and Richardson (2003, hereafter referred to as C&R) developed a near-Earth ICME list for the time period 1996 through 2002. In compiling this list, they first identified possible ICMEs based on the temperature criterion described above, then incorporated complementary signatures such as reduced fluctuations of the magnetic field, shocks, compositional anomalies, and Forbush decreases. They did not take into account the helium abundance or bi-directional electrons. A comparison of the C&R list with ours shows that about 85% of the events on our list are also on their list (although the ICME boundaries often differ). Our criteria yields about 50% less events than on the C&R list. Again, we mark the events that are identified as MCs on the on-line WIND and ACE lists.

4. Propagation of ICMEs

The ICME list is used to explore ICME evolution in a statistical sense; we discuss mainly the plasma and magnetic field data. ICMEs should bear some similarities to MCs in their dynamics and energetics but may also have significant differences. MCs are better organized in terms of magnetic structure and thus may not be appreciably deformed during propagation. We also compare the ICME evolution with that of the solar wind, which could reveal how the ejecta interacts with the ambient interplanetary medium. Consequently, this section provides observational constraints for theoretical models of ICMEs.

4.1. Expansion of the radial width

In a typical ICME the leading edge moves faster than the trailing edge, which results from the radial expansion of the ICME. We define the expansion speed as the speed difference between the forward and trailing edges of the ICME. Using the method in Section 3, we obtain the expansion speeds for each ICME which are shown in Fig. 3. The average expansion speed changes very slowly with distance, from 65 to 45 $\mathrm{km\,s^{-1}}$ between 0.3 and 5.4 AU, as shown by the power-law fit

$$\Delta v(R) = (57.48 \pm 5.00) \times R^{(-0.12\pm0.13)}\,(\mathrm{km\,s^{-1}}). \quad (2)$$

Although the distribution of Δv is broad near the Sun, the scatter decreases quickly with distance. Since the

Table 1
ICMEs observed by Helios 1 and 2, Ulysses, WIND and ACE

Spacecraft	Year	Start (DOY)	Duration (h)	Distance (AU)	Heliolongitude (deg)	Heliolatitude (deg)	$\langle v \rangle$ (km s^{-1})	Radial width (AU)	Note
Helios 1	1975	6.07	18.09	0.93	352.17	−2.65	543.77	0.24	
	1977	29.43	23.83	0.95	323.15	−2.08	454.28	0.26	MC [a]
		33.93	5.19	0.93	322.00	−2.49	312.11	0.04	
		78.75	6.36	0.57	329.41	−6.90	453.54	0.07	MC
		100.26	8.44	0.32	32.21	−2.85	473.00	0.10	
		268.33	19.59	0.57	145.10	−6.85	734.71	0.35	MC
		335.70	22.73	0.75	323.66	4.90	416.37	0.23	MC
	1978	5.64	20.38	0.96	319.77	1.39	488.74	0.24	
		61.08	28.83	0.87	304.63	−3.60	442.62	0.31	MC
		103.84	4.92	0.44	330.93	−7.14	367.66	0.04	
		146.33	20.48	0.60	126.38	6.53	394.48	0.19	
		169.93	24.15	0.83	135.69	3.91	359.28	0.21	
		290.63	24.90	0.48	140.09	−7.22	456.13	0.27	
		342.20	21.71	0.66	305.24	5.90	330.76	0.17	
		363.09	59.96	0.85	308.91	3.60	670.97	0.97	MC
	1979	3.23	9.52	0.88	308.35	3.07	485.76	0.11	
		12.00	9.75	0.92	306.71	2.22	392.18	0.09	
		31.45	34.32	0.98	301.30	0.45	421.11	0.35	
		36.88	23.05	0.98	299.60	−0.03	328.38	0.18	
		40.37	36.53	0.98	298.50	−0.34	412.12	0.36	
		58.54	43.31	0.95	293.11	−1.94	518.19	0.54	MC
		63.23	17.59	0.94	291.93	−2.36	526.17	0.22	
		76.21	6.91	0.87	289.59	−3.58	379.80	0.06	
		84.14	10.73	0.82	289.15	−4.36	493.28	0.13	
		89.56	24.18	0.77	289.52	−4.92	376.92	0.22	
		105.36	7.45	0.62	295.93	−6.54	712.67	0.13	
		176.21	7.35	0.75	120.02	4.90	522.00	0.09	
		346.21	27.91	0.53	279.31	7.04	364.73	0.24	
	1980	69.88	4.28	0.97	279.09	−1.58	323.65	0.03	
		90.42	17.42	0.88	274.77	−3.47	484.49	0.20	MC
		92.33	10.70	0.87	274.57	−3.66	379.81	0.10	
		121.26	13.56	0.61	281.71	−6.59	314.22	0.10	
		172.45	7.14	0.54	92.25	6.96	385.38	0.07	MC
		183.85	5.32	0.67	102.65	5.77	397.33	0.05	
		190.12	34.15	0.74	105.26	5.06	487.99	0.40	
		204.07	13.95	0.85	106.98	3.55	364.82	0.12	
		217.05	12.21	0.92	105.74	2.27	396.46	0.12	
	1981	27.59	11.58	0.85	278.24	3.61	601.00	0.17	
		28.44	16.94	0.85	278.18	3.53	533.47	0.22	
		30.92	12.49	0.87	277.94	3.27	427.64	0.13	
		101.03	12.60	0.90	260.46	−3.12	382.47	0.12	
		104.08	44.24	0.88	260.05	−3.41	548.63	0.58	
		131.57	17.12	0.65	264.30	−6.20	848.46	0.35	MC
		134.18	48.38	0.62	266.06	−6.46	626.37	0.73	
		146.08	31.70	0.47	281.19	−7.23	474.54	0.36	MC
		170.15	11.87	0.34	29.79	4.80	601.63	0.17	MC
		327.16	14.01	0.59	83.71	−6.72	565.10	0.19	
	1982	38.83	20.65	0.82	263.11	4.04	435.66	0.22	
Helios 2	1977	29.87	4.22	0.98	350.73	−5.10	487.97	0.05	
		83.41	9.65	0.63	348.06	−7.19	414.52	0.10	
		95.80	3.79	0.47	2.82	−6.06	460.19	0.04	
	1978	4.30	26.14	0.94	354.55	−2.76	562.54	0.35	MC
		6.01	14.37	0.95	354.07	−2.90	571.19	0.20	MC
		30.25	13.12	0.98	346.32	−4.70	573.93	0.18	
		37.71	45.80	0.97	343.88	−5.18	375.67	0.41	MC
		61.45	9.82	0.88	337.80	−6.48	440.51	0.10	
		66.20	6.68	0.85	337.18	−6.69	395.72	0.06	
		68.07	27.27	0.84	337.03	−6.77	520.53	0.34	
		100.15	7.88	0.50	352.45	−6.46	476.76	0.09	
		106.78	8.33	0.41	6.86	−4.87	429.02	0.09	

Table 1 (*continued*)

Spacecraft	Year	Start (DOY)	Duration (h)	Distance (AU)	Heliolongitude (deg)	Heliolatitude (deg)	$\langle v \rangle$ (km s^{-1})	Radial width (AU)	Note
		108.89	7.30	0.38	13.55	−4.00	717.80	0.13	
		348.72	9.77	0.77	351.35	0.25	469.94	0.11	
		349.47	9.09	0.77	351.42	0.14	534.56	0.12	
		365.17	43.82	0.89	350.44	−1.73	576.99	0.61	
	1979	6.62	13.24	0.92	349.07	−2.36	442.69	0.14	
		23.29	25.82	0.98	344.27	−3.75	411.54	0.26	
		31.49	28.20	0.98	341.57	−4.34	545.75	0.37	
		35.15	23.18	0.98	340.36	−4.59	421.91	0.24	
		43.23	8.94	0.98	337.72	−5.11	395.39	0.09	
		50.85	18.22	0.96	335.38	−5.56	447.06	0.20	
		93.09	18.54	0.67	333.30	−7.24	438.26	0.20	MC
		96.49	7.06	0.64	335.15	−7.20	540.82	0.09	
		364.96	24.83	0.85	344.75	−0.97	387.74	0.23	MC
	1980	13.36	14.56	0.92	342.45	−2.36	469.65	0.16	
Ulysses	1990	360.21	67.00	1.54	20.30	−0.50	351.81	0.57	
	1991	16.71	50.00	1.77	31.10	−1.80	402.92	0.48	
		57.71	23.00	2.22	45.20	−3.30	466.28	0.26	
		75.21	55.00	2.41	49.60	−3.70	461.29	0.61	
		88.50	100.00	2.57	52.60	−4.00	640.94	1.54	
		149.00	60.00	3.18	62.70	−4.80	591.65	0.85	
		156.00	62.00	3.25	63.60	−4.90	460.41	0.69	
		207.00	124.00	3.75	69.30	−5.30	385.76	1.15	
		253.33	71.00	4.16	73.30	−5.50	481.94	0.82	
		321.62	66.00	4.74	78.10	−5.80	566.20	0.90	
	1992	12.00	96.00	5.19	81.10	−6.00	553.10	1.28	
		67.21	43.00	5.40	82.50	−7.50	445.05	0.46	
		73.33	203.00	5.40	82.50	−7.80	484.95	2.37	
		173.42	76.00	5.35	83.40	−12.70	385.02	0.70	
	1993	11.50	108.00	5.04	85.40	−23.50	472.44	1.23	
		49.33	59.00	4.95	85.90	−25.60	574.45	0.82	
	1996	289.00	144.00	4.46	76.60	24.30	627.51	2.17	ICME[b]
		346.42	134.00	4.65	77.40	20.40	504.35	1.63	ICME
	1998	83.00	103.00	5.41	81.90	−4.90	364.40	0.90	ICME
		169.00	103.00	5.40	82.70	−9.10	455.06	1.13	ICME
		191.00	79.00	5.39	82.90	−10.20	496.98	0.94	ICME
		218.50	105.00	5.37	83.10	−11.60	406.66	1.03	ICME
		260.71	88.00	5.33	83.50	−13.60	354.80	0.75	ICME
		283.00	129.00	5.31	83.70	−14.70	396.03	1.23	ICME
		310.62	112.00	5.28	84.00	−16.20	429.61	1.16	ICME
		342.62	76.00	5.24	84.30	−17.80	515.26	0.94	ICME
	1999	22.71	64.00	5.17	84.70	−20.20	438.42	0.68	ICME
		163.50	153.00	4.85	86.40	−28.10	433.37	1.60	ICME
		231.00	36.00	4.66	87.40	−32.30	394.87	0.34	ICME
		243.00	98.00	4.61	87.60	−33.10	513.98	1.21	ICME
	2000	199.83	76.00	3.14	100.70	−62.70	364.78	0.67	
		223.83	64.00	3.00	104.00	−66.00	435.88	0.67	ICME
	2001	94.00	57.00	1.45	255.00	−31.40	393.82	0.54	
		99.50	28.00	1.43	255.90	−27.60	427.22	0.29	
		110.50	84.00	1.39	257.50	−19.80	601.38	1.22	
		131.33	40.00	1.35	260.40	−3.90	511.07	0.49	
		157.33	64.00	1.35	264.00	16.60	418.87	0.65	ICME
		161.42	33.00	1.35	264.60	19.70	380.14	0.30	
		312.83	40.00	2.22	34.20	76.60	783.57	0.75	ICME
	2002	125.21	105.00	3.37	70.70	46.10	355.02	0.90	ICME
		165.50	144.00	3.60	72.30	41.30	601.65	2.08	ICME
		198.50	26.00	3.75	73.30	38.00	529.55	0.33	ICME
		222.50	96.00	3.88	74.00	35.50	442.51	1.02	
WIND/ACE[c]	1995	292.02	23.04	1.00	309.60	5.60	405.15	0.22	MC[d]
	1996	123.73	18.00	1.01	146.60	−4.00	360.91	0.16	
	1997	101.31	6.00	1.00	125.20	−5.90	465.07	0.07	

Table 1 (*continued*)

Spacecraft	Year	Start (DOY)	Duration (h)	Distance (AU)	Heliolongitude (deg)	Heliolatitude (deg)	$\langle v \rangle$ (km s^{-1})	Radial width (AU)	Note
		135.44	24.96	1.01	158.20	−2.70	475.85	0.29	MC[d]
		300.52	23.04	0.99	317.60	4.90	449.08	0.25	
		312.10	26.16	0.99	329.60	3.70	383.82	0.24	MC[d,e]
		326.73	18.00	0.99	343.60	2.10	506.79	0.22	MC[d]
	1998	7.10	28.08	0.98	30.30	−3.70	384.04	0.26	MC[d,e]
		63.70	33.53	0.99	87.20	−7.20	339.35	0.27	MC[d,e]
		73.90	14.40	0.99	97.30	−7.20	404.24	0.14	
		122.30	40.73	1.01	145.60	−4.10	518.20	0.51	MC[d,e]
		126.10	11.93	1.01	149.50	−3.70	468.71	0.13	
		127.00	21.60	1.01	150.50	−3.60	471.73	0.25	
		140.00	12.00	1.01	163.00	−2.10	389.53	0.11	
		176.10	19.13	1.02	197.20	2.10	438.45	0.20	MC[d]
		213.50	36.00	1.01	232.40	5.70	412.06	0.36	MC[e]
		253.80	12.00	1.01	271.10	7.20	337.45	0.10	
		268.30	36.00	1.00	285.90	7.00	633.56	0.55	MC[d,e]
		272.10	24.00	1.00	289.80	6.80	414.25	0.24	
		312.00	72.00	0.99	329.60	3.70	469.26	0.81	MC[d,e]
		334.85	7.20	0.99	351.60	1.10	466.92	0.08	
	1999	49.50	52.80	0.99	73.00	−6.90	531.13	0.67	MC[d]
		69.50	38.33	0.99	93.30	−7.20	416.02	0.38	MC[e]
		106.90	19.20	1.00	130.10	−5.60	412.95	0.19	MC[d,e]
		111.20	33.53	1.00	135.00	−5.10	488.84	0.39	MC[e]
		153.10	9.53	1.01	175.30	−0.60	373.16	0.09	
		178.90	9.60	1.02	199.10	2.40	685.29	0.16	
		186.70	23.93	1.02	206.60	3.30	366.02	0.21	
		211.80	12.00	1.02	230.50	5.60	612.79	0.18	
		212.80	12.00	1.02	231.40	5.70	562.74	0.16	
		221.30	28.80	1.01	240.10	6.30	347.70	0.24	MC[d]
		265.80	40.80	1.00	282.90	7.10	522.06	0.51	
		334.50	14.40	0.99	351.60	1.10	363.82	0.13	
	2000	43.23	18.00	0.99	66.90	−6.70	562.40	0.24	MC[d,e]
		52.50	24.00	0.99	76.10	−7.00	380.92	0.22	MC[d,e]
		70.00	19.20	0.99	94.30	−7.20	380.92	0.18	
		89.80	64.73	1.00	113.30	−6.70	413.21	0.64	
		98.20	12.00	1.00	122.20	−6.10	592.29	0.17	
		123.90	60.00	1.01	146.60	−4.00	473.54	0.68	MC[e]
		135.10	59.93	1.01	158.20	−2.70	433.30	0.62	MC[e]
		144.50	74.40	1.01	166.80	−1.70	558.41	1.00	
		157.10	45.53	1.01	179.10	−0.10	449.15	0.49	
		161.00	43.20	1.02	182.90	0.40	574.26	0.60	
		163.30	12.00	1.02	184.80	0.60	512.75	0.15	MC[e]
		165.50	36.00	1.02	186.70	0.90	440.16	0.38	MC[e]
		171.90	7.13	1.02	192.40	1.60	387.01	0.07	
		173.80	14.40	1.02	194.30	1.80	404.15	0.14	
		176.10	45.53	1.02	197.20	2.10	501.10	0.55	
		193.10	9.53	1.02	213.30	4.00	436.49	0.10	
		194.00	26.40	1.02	214.20	4.10	503.02	0.32	MC[e]
		198.60	33.53	1.02	218.00	4.50	666.27	0.54	
		203.80	24.00	1.02	222.80	4.90	432.15	0.25	
		205.50	62.40	1.02	224.70	5.10	357.54	0.54	
		210.60	47.93	1.02	229.50	5.50	452.07	0.52	MC[d,e]
		223.80	16.80	1.01	242.00	6.40	428.88	0.17	MC[e]
		225.20	40.80	1.01	243.90	6.50	570.72	0.56	MC[d,e]
		253.10	26.27	1.01	271.10	7.20	409.26	0.26	
		262.00	76.80	1.00	280.00	7.10	615.89	1.14	MC[d]
		277.50	40.80	1.00	294.80	6.60	405.04	0.40	MC[d,e]
		287.50	28.80	1.00	304.70	6.00	406.48	0.28	MC[d,e]
		332.30	12.00	0.99	349.60	1.30	599.93	0.17	MC[e]
		333.90	24.00	0.99	350.60	1.20	515.68	0.30	
		339.00	12.00	0.99	356.70	0.40	368.54	0.11	
	2001	63.60	14.40	0.99	87.20	−7.20	436.56	0.15	
		79.02	28.08	1.00	103.30	−7.00	396.65	0.27	MC[d]

Table 1 (*continued*)

Spacecraft	Year	Start (DOY)	Duration (h)	Distance (AU)	Heliolongitude (deg)	Heliolatitude (deg)	$\langle v \rangle$ (km s^{-1})	Radial width (AU)	Note
		86.90	74.40	1.00	110.30	−6.80	522.13	0.93	
		90.23	83.04	1.00	114.30	−6.60	593.11	1.19	
		102.30	23.93	1.00	126.10	−5.90	638.97	0.37	
		103.70	16.80	1.00	127.10	−5.80	699.41	0.28	
		109.80	16.73	1.00	133.00	−5.30	392.25	0.16	
		118.60	86.40	1.01	141.80	−4.50	500.15	1.04	
		127.70	16.80	1.01	150.50	−3.60	362.41	0.15	
		129.50	33.60	1.01	152.40	−3.40	430.94	0.35	
		148.40	48.00	1.01	170.60	−1.20	423.28	0.49	MC[d]
		190.20	33.60	1.02	210.40	3.70	407.86	0.33	MC[d]
		237.30	24.00	1.01	255.50	7.00	384.62	0.22	
		267.31	35.04	1.00	284.90	7.00	412.77	0.35	
		275.70	23.93	1.00	292.80	6.70	508.68	0.29	
		278.30	12.00	1.00	295.80	6.50	396.03	0.11	
		285.10	7.20	1.00	302.70	6.10	555.28	0.10	
		288.50	33.60	1.00	305.70	5.90	386.59	0.31	
		294.90	84.00	1.00	311.60	5.40	476.15	0.96	
		302.70	50.33	0.99	319.60	4.70	361.44	0.44	
		329.00	55.20	0.99	346.60	1.70	579.70	0.77	
		342.50	19.20	0.98	359.70	0.00	406.43	0.19	
		362.20	21.53	0.98	19.90	−2.50	358.55	0.19	
	2002	59.70	45.60	0.99	83.20	−7.20	381.51	0.42	
		80.70	14.40	1.00	104.30	−7.00	438.34	0.15	
		83.50	28.80	1.00	107.30	−6.90	436.21	0.30	MC[d]
		95.40	21.60	1.00	119.20	−6.30	388.32	0.20	
		103.00	9.60	1.00	127.10	−5.80	405.99	0.09	
		107.90	38.40	1.00	131.00	−5.50	492.04	0.45	
		146.20	14.40	1.01	168.70	−1.40	438.23	0.15	
		202.50	16.73	1.02	221.90	4.80	508.00	0.20	
		213.60	14.27	1.01	232.40	5.70	465.51	0.16	MC[d]
		231.80	52.80	1.01	249.70	6.80	451.22	0.57	
		252.40	36.00	1.01	270.10	7.20	429.23	0.37	
		276.70	47.93	1.00	293.80	6.60	404.39	0.47	
		296.60	9.60	1.00	313.60	5.30	423.27	0.10	

[a]The events indicated for Helios 1 and 2 were identified as MCs by Bothmer and Schwenn (1998).
[b]The events indicated for Ulysses can be confirmed by the Ulysses ICME list.
[c]The ICMEs listed for WIND and ACE were observed by both spacecraft.
[d]Events recognized as MCs in the WIND list.
[e]Events recognized as MCs in the ACE list.

average expansion speed varies little with distance inside 5.4 AU, the radial expansion of ICMEs can be considered to be in quasi-equilibrium, consistent with the theoretical picture of Chen (1996). Fig. 4 displays the radial width of the events listed in Table 1 versus the heliocentric distance and the best fit of a power law to the data:

$$S(R) = (0.25 \pm 0.01) \times R^{(0.92\pm0.07)}\,(\mathrm{AU}). \quad (3)$$

The radial expansion causes the radial width of ICMEs to increase with distance: the average radial width is about 0.25 AU near Earth and increases to about 1.1 AU at 5 AU. A linear fit to the ICME width gives $S = (0.20 \pm 0.01) \times R + (0.11 \pm 0.03)$, which may give us an estimate of the diameter of ICMEs close to the Sun. Bothmer and Schwenn (1998) found a similar scaling relation, $S(R) = (0.24 \pm 0.01) \times R^{(0.78\pm0.10)}$, in a statistical study of MCs between 0.3 and 4.2 AU. A theoretical calculation yielded $S(R) \sim R^{0.88}$ for ICMEs between 0.3–5 AU (Chen, 1996). These results are consistent with those reported here.

The expansion of ICMEs may affect the average physical conditions within the ICME plasma, such as the density N, bulk speed v, temperature T and magnetic field strength B. The radial evolution of these parameters is shown in Fig. 5. The solid lines represent the profiles that best fit the data:

$$N(R) = (6.16 \pm 0.30) \times R^{(-2.32\pm0.07)}\,(\mathrm{cm}^{-3}), \quad (4)$$

$$v(R) = (458.40 \pm 6.27) \times R^{(-0.002\pm0.02)}\,(\mathrm{km\,s}^{-1}), \quad (5)$$

$$T(R) = (35401.1 \pm 1328.3) \times R^{(-0.32\pm0.06)}(\mathrm{K}), \quad (6)$$

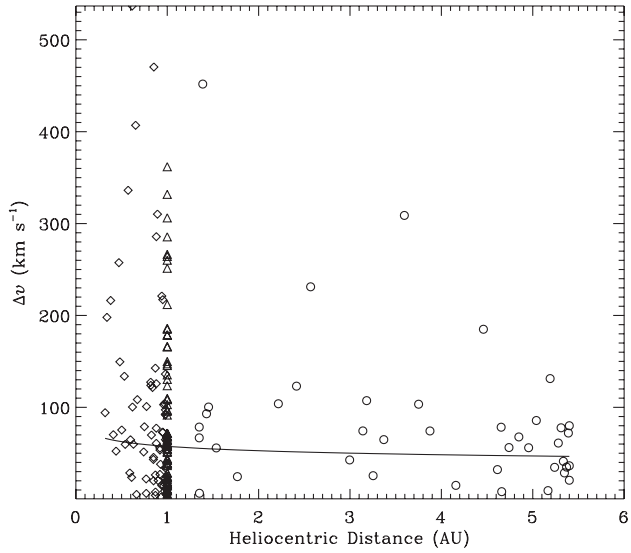

Fig. 3. Expansion speeds of ICMEs observed by Helios 1 and 2 (diamonds), WIND and ACE (triangles) and Ulysses (circles). The solid line shows a power-law fit to the data.

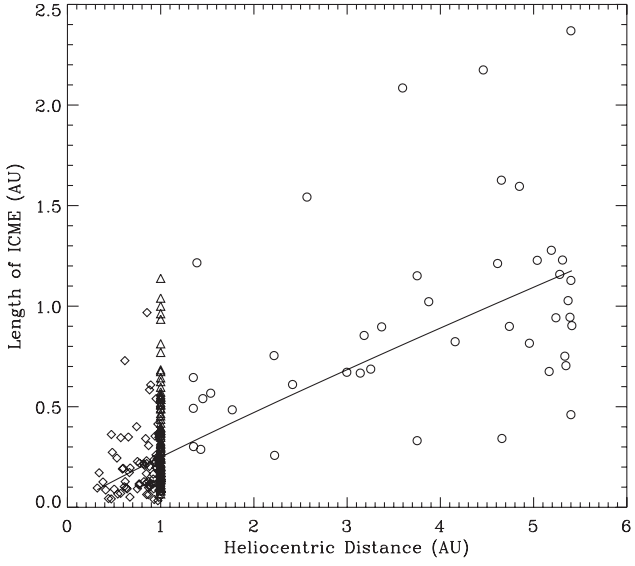

Fig. 4. Radial widths of ICMEs observed by Helios 1 and 2 (diamonds), WIND and ACE (triangles) and Ulysses (circles). The solid line is a power-law fit to the data.

$$B(R) = (7.35 \pm 0.40) \times R^{(-1.40 \pm 0.08)}\,(\mathrm{nT}). \quad (7)$$

According to the fits, the average density inside ICMEs is about $6.2\,\mathrm{cm}^{-3}$ at 1 AU, slightly lower than the background solar wind density, $7\,\mathrm{cm}^{-3}$. In addition, the density decreases faster with radial distance than in the solar wind, where the density falls off as R^{-2} out to 70 AU (Richardson et al., 2004). The lower density compared to the ambient solar wind is in agreement with ICME expansion models. The second panel in

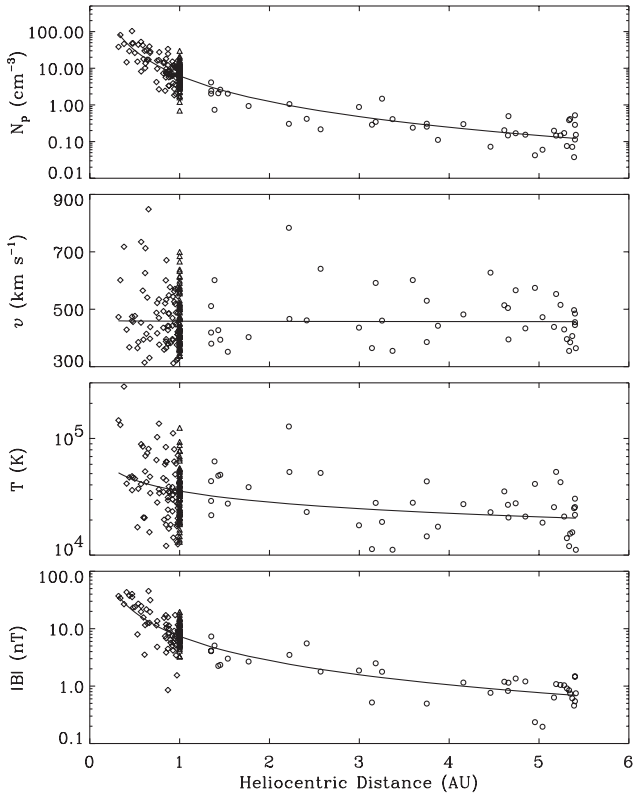

Fig. 5. Average plasma properties within ICMEs observed by Helios 1 and 2 (diamonds), WIND and ACE (triangles) and Ulysses (circles). From top to bottom are the proton density, the proton bulk speed, the proton temperature, and the magnitude of the magnetic field. Solid lines show power-law fits to the data.

Fig. 5 shows that the average speed of the ejecta is about $450\,\mathrm{km\,s}^{-1}$ and remains constant over the whole distance. This value is comparable to the average solar wind speed near Earth, i.e., $440\,\mathrm{km\,s}^{-1}$. The third panel shows how the temperature inside ICMEs evolves with distance. The best fit gives an average temperature of 3.5×10^4 K at 1 AU, well below the typical solar wind temperature, 9.5×10^4 K. This result is expected since the ICME identification is based on the low temperature criterion. However, the temperature decreases slowly with distance compared with the R^{-1} dependence of the temperature of the average solar wind, which was not expected. The slower decrease of temperature with distance implies substantial heating of the ejecta; otherwise the temperature would fall off faster than that of the background medium due to adiabatic cooling resulting from the ICME expansion. The bottom panel shows that the average magnetic field magnitude in ICMEs is 7.4 nT at 1 AU, which is larger than the average solar wind magnetic field magnitude of 6.3 nT. The higher magnetic field, which contributes most of the internal pressure inside ICMEs, could contribute to the radial expansion of ICMEs when the magnetic field deviates from the force-free configuration (Suess, 1988;

Cargill et al., 1997). The equatorial magnetic field in the ambient solar wind decreases as $R^{-1.1}$, which is slower than in ICMEs, again consistent with ICME expansion.

ICMEs are expected to co-move with the solar wind at large heliocentric distances. To test this hypothesis, we compare the standard deviation of speed between ICMEs and the solar wind, based on the observations of Ulysses outside 5 AU. To avoid heliolatitude effects, we choose the time interval from 1997.5 through 1998.2, which corresponds to a distance range of 5.15–5.4 AU (see Fig. 1) The standard deviation of the solar wind speed is about 23.2 km s^{-1} in this time period, while those for individual ICMEs observed at 5.15–5.4 AU range from 7.6 to 42 km s^{-1}, with 77% (10 out 13) smaller than the solar wind level. This result is in agreement with our expectation.

4.2. Thermodynamic structure

Ideal MHD equations have been used to model the dynamic behavior of coronal, solar wind and some space weather events. An outstanding issue is the energy transport process, which is extremely complicated. To retain a qualitative aspect of this heating while keeping the physics simple, a polytropic gas is often assumed and the energy transport is then described by a polytropic index γ. Since the polytropic process, in theory, is reversible, this assumption is referred to as the isentropic case. In most models, the value of γ is set equal to $\frac{5}{3}$, the adiabatic case. In simulating CMEs different values of γ are sometimes used, often without substantiation. In this work we empirically determine the value of γ that governs the propagation and expansion of ICMEs.

For an ideal, isotropic fluid, the polytropic equation is given by

$$TN^{1-\gamma} = \text{constant}, \tag{8}$$

where T and N are the temperature and the number density of the fluid, respectively. Theoretically, if γ is less than 1, the temperature will grow with distance; for an isothermal expansion, $\gamma = 1$, the temperature will remain constant; if γ is greater than 1 but less than $\frac{5}{3}$, the temperature will decrease as the ejecta expand but not cool rapidly enough to be considered as an adiabatic process (which implies that heat must be supplied to the ejecta during expansion). Theoretical calculations by Chen and Garren (1993) showed that the temperature of flux ropes decreases to a few degrees Kelvin at 1 AU if $\gamma = \frac{5}{3}$ is assumed, while the average observed temperature is 3.5×10^4 K. Hence, we would expect $1 < \gamma < \frac{5}{3}$ for ICMEs.

One way to derive the value of γ is to directly fit the temperature and density data for individual ICMEs using Eq. (8). The observations of Helios and Ulysses allow us to investigate whether the index is constant with distance as assumed by most MHD models. The observations of WIND and ACE enable us to investigate the variation of γ with the solar activity level. Fig. 6 displays the polytropic indices for protons and electrons, respectively. To the best of our knowledge, a comprehensive Helios electron data set is not available. The electron index from the Helios spacecraft is thereby absent in the lower left panel. Electron data points are also sporadic for WIND and ACE. Fig. 6 shows no clear distance or solar activity level dependence of the polytropic indices, hence they can be considered as constant. The average value of the index for protons, γ_p, is about 1.03, which indicates that the ICME expansion is isothermal. For ICME electrons, $\gamma_e \sim 0.73$, suggesting that the temperature of electrons grows with distance. For comparison, the solar wind has $\gamma_p \sim 1.5$ (Totten et al., 1995) and $\gamma_e \sim 1.2$ (Sittler and Scudder, 1980), while MCs have $\gamma_p = 1.1$–1.3 (Osherovich et al., 1993c) and $\gamma_e \sim 0.5$ (Sittler and Burlaga, 1998). Therefore, $\gamma_e < 1$ is a commonly reported feature of ICMEs. However, treatment of the electrons is more complicated because of the core and halo components and their anisotropy. As proved by Scudder (1992), a polytrope relation with $\gamma < 1$ results from non-Maxwellian distributions of the gas particles. Thus the direct application of Eq. (8) to the ICME electrons may be questionable. The characteristics of the polytropic indices for protons and the ejecta as a whole will be discussed later.

To give a clear picture of the evolution of the electrons, we show in Fig. 7 the electron temperature and density as a function of distance determined from the observations of Ulysses. The best fits to the data are:

$$N_e(R) = (4.57 \pm 1.27) \times R^{(-2.03\pm0.21)}\,(\text{cm}^{-3}), \tag{9}$$

$$T_e(R) = (149690.3 \pm 24600.2) \times R^{(-0.64\pm0.12)}\,(\text{K}). \tag{10}$$

The electron temperature, T_e, decreases slightly faster than that of protons; in addition, there is not a clear anticorrelation between T_e and N_e. The radial evolution of electron and proton densities are very similar (see Fig. 5), consistent with the fact that they are driven by the same expanding structure.

As discussed in Section 3, ICME boundaries are often difficult to determine. Hence, some ICMEs may contain different flux tubes which have different specific entropies. Variations in the entropy from one flux rope to another will affect the accuracy of our derivation of the polytropic index. An empirical treatment proposed by Totten et al. (1995) may be more appropriate. Differentiating Eq. (8) with respect to R and assuming $T \sim R^{-\alpha}, N \sim R^{-\delta}$, we obtain the following relation:

$$\gamma_p = 1 + \frac{\alpha}{\delta}. \tag{11}$$

An assumption of this equation is that γ is constant with distance, as shown by Fig. 6. Substituting the values of α and δ (refer to Eqs. (6) and (4)) into the above equation

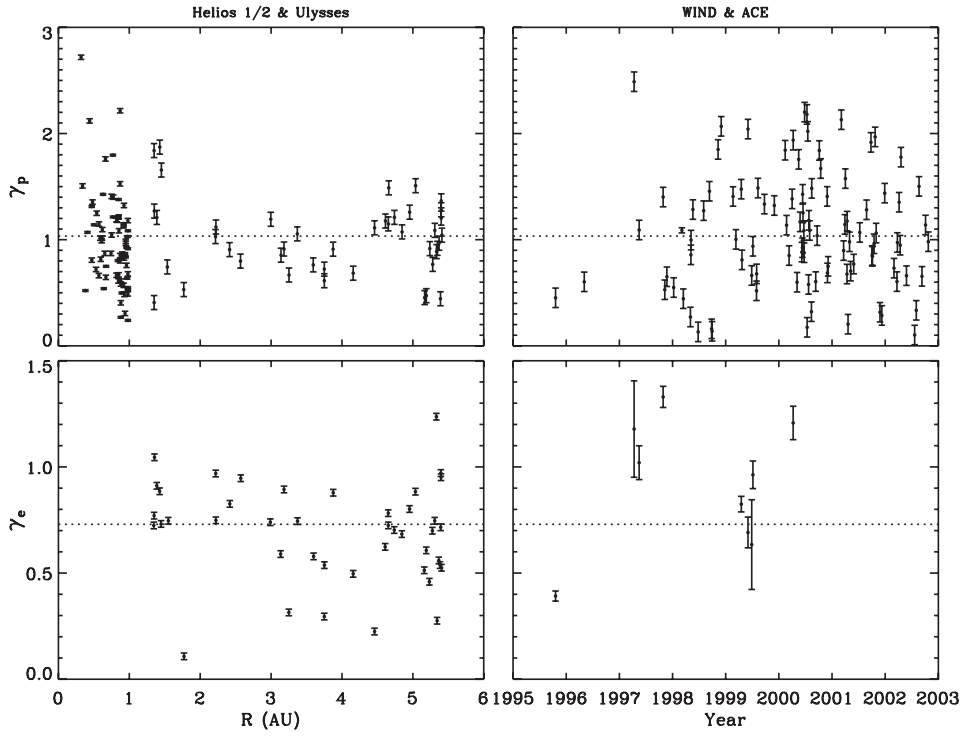

Fig. 6. Distance dependence (left panels) and solar cycle variation (right panels) for polytropic indices of protons (upper panels) and electrons (lower panels) within individual ICMEs. Error bars indicate the 3σ confidence levels. The dotted lines show the overall average values. Data in the left panels are from Helios 1 and 2 and Ulysses; data in the right panels are from WIND and ACE.

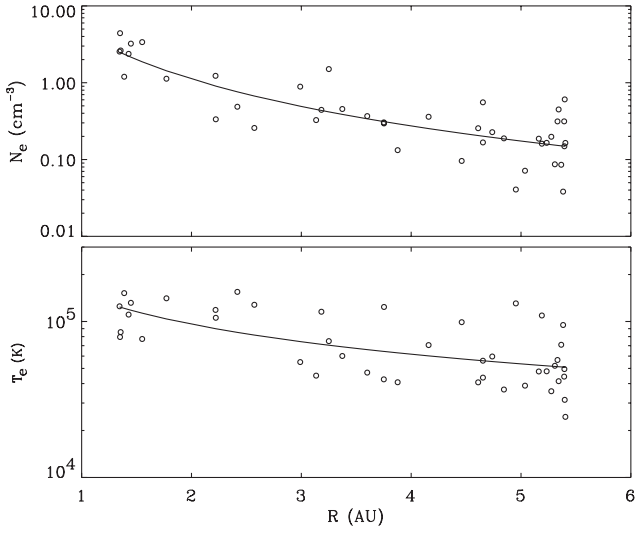

Fig. 7. Evolution of the average electron density (upper panel) and temperature (lower panel) inside ICMEs observed by Ulysses. The solid lines show the best power-law fits to the data.

gives $\gamma_p = 1.14 \pm 0.03$, close to the value in MCs ($\gamma_p = 1.1$–1.3).

Note that a single-fluid treatment of the thermodynamic structure is not complete without considering the electron component. In addition, the magnetic field significantly contributes to the total internal pressure. Therefore we have to consider the contributions from electrons and the magnetic field. We examine the two cases separately to find how these components affect the values of γ; to do so we need some pre-knowledge about the percentage contribution of the different components to the total pressure. This information is provided by the electron-to-proton pressure ratio $\chi = N_e kT_e/N_p kT_p$ and the plasma beta $\beta = (N_e kT_e + N_p kT_p)/B^2/2\mu_0$, where k is Boltzmann's constant and μ_0 is the permeability of free space. The observations show that the pressure ratio χ and the plasma β do not depend on distance or solar activity levels, similar to the case of γ displayed in Fig. 6. The average value of χ is about 3.25, which shows that the electron contribution to the total pressure is larger than that of the protons. $\beta \sim 0.92$, showing that the most probable state of the ICME plasma is one of equipartition between the thermal pressure and the magnetic pressure. The plasma-beta for protons, by definition, is $\beta_p = \beta/(\chi + 1)$, from which we obtain $\beta_p \sim 0.22$, consistent with the fact that low β_p is generally present in the ICME plasma.

We can now assess the effect of the electrons and the magnetic field on γ. We first take into account the electron pressure. The polytropic equation is now given:

$$\frac{N_e kT_e + N_p kT_p}{(N_p + N_e)^{\gamma}} = \text{constant}. \tag{12}$$

Assuming $N_p = N_e$ (due to charge neutrality of the ICME plasma) and taking the derivative with respect to R, we obtain

$$\gamma = \frac{(\alpha_e + \delta_e)\chi + (\alpha_p + \delta_p)}{(\chi + 1)\delta_p}, \quad (13)$$

where we used the definition of χ and assumed $T_e \sim R^{-\alpha_e}$ and $N_e \sim R^{-\delta_e}$, similar to the proton case. The values of δ_p, α_p, δ_e and α_e can be obtained from Eqs. (4), (6), (9) and (10) respectively. The outcome is $\gamma \sim 1.15$. It is surprising that γ is not modified by including the electron pressure. Since electrons are the major contributor to the thermal pressure, we would expect a significant change in the value of γ, which was not found. Now we include the magnetic pressure, and the polytrope relation has the following form:

$$\frac{N_e k T_e + N_p k T_p + B^2/2\mu_0}{(N_p + N_e)^\gamma} = \text{constant}. \quad (14)$$

Let $B \sim R^{-\lambda}$, again assume $N_p = N_e$ and take the radial derivative. The new expression of γ is

$$\gamma = \frac{(\alpha_e + \delta_e)\chi\beta + (\alpha_p + \delta_p)\beta + 2\lambda}{(\chi\beta + \beta + 1)\delta_p}, \quad (15)$$

which yields $\gamma \sim 1.16$. Therefore, inclusion of neither electrons nor the magnetic field alters the value of γ. The specific cause is that $\alpha_e + \delta_e \sim \alpha_p + \delta_p \sim 2\lambda$, which cancels the terms comprised by χ and β in Eqs. (13) and (15); more specifically, the value of γ seems independent of χ and β. This implies that the physical conditions within ICMEs are such that the polytropic index is fixed. This result contrasts with the case of the solar wind, for which $\gamma_p \sim 1.46$ which changes to 1.58 when the magnetic pressure is included (Totten et al., 1995). Further investigations are needed to disclose the underlying physics responsible for this feature of ICMEs.

As stated above, the result $\gamma \sim 1.15$ indicates that significant heating occurs in ICMEs and that the plasma behaves more like an isothermal than an adiabatic gas. With the assumption $\gamma = \frac{4}{3}$, Gibson and Low (1998) constructed an analytic solution describing the expulsion of a 3D CME out of the solar corona, while Chen (1996) employed $\gamma = 1.2$ in his theoretical treatment of the ICME initiation and propagation. Krall et al. (2000) found that the results from the Chen (1996) model with $\gamma = 1.2$ can reproduce key features of MCs over the range of 0.4–5 AU. These values are close to that determined here. γ close to unity implies that thermal conduction from the Sun may account for the heating. If the footpoints of ICMEs are rooted in the photosphere (as generally believed) which has a lower temperature than the ejecta, heat cannot be directly transmitted from the Sun. However, it seems reasonable to speculate that the mechanism responsible for heating the corona might also contribute to the heating of ICMEs. Without giving a detailed description of the heating mechanism, Kumar and Rust (1996) suggested that the heating may result from the local magnetic dissipation and their calculations showed that at least 58% of the lost magnetic energy is converted to heat. As evidenced by Kahler and Reames (1991), energetic particles produced by solar flare eruption may enter MCs along the field lines; the heating mechanism may involve energetic particles or Alfvén waves coming from the solar atmosphere. Streaming electrons are often associated with ICMEs and may also contribute to the heating.

4.3. Properties near the Earth

ICMEs observed by WIND and ACE provide a detailed picture of the average features of ICMEs at Earth. The occurrence rate and average physical conditions of ICMEs have a solar cycle dependence.

Fig. 8 shows the distributions of ICMEs at 1 AU, CMEs observed by LASCO (http://cdaw.gsfc.nasa.gov/cme_list), and sunspots over solar cycle 23 (http://spidr.ngdc.noaa.gov/spidr). Note that the numbers are expressed as a five-solar-rotation running mean. The vertical bars in the upper panel represent the effect of

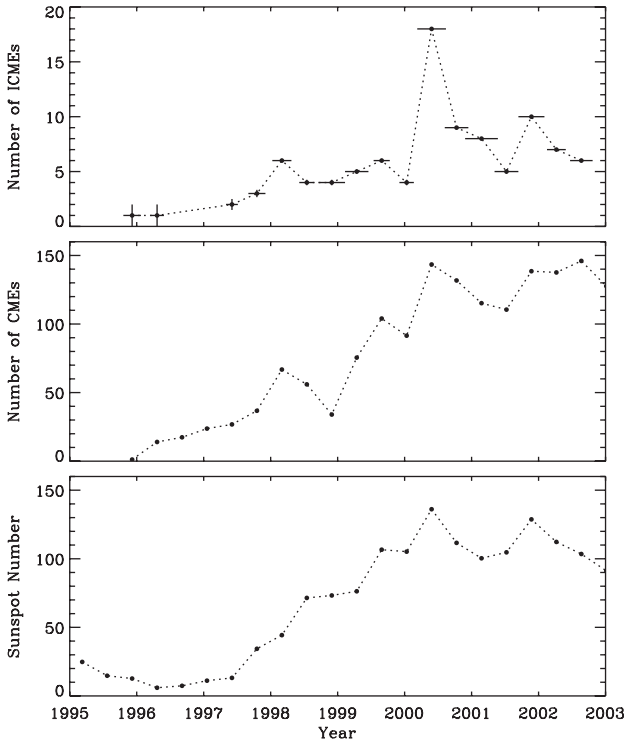

Fig. 8. The number of ICMEs (upper panel) at 1 AU, the number of CMEs observed by LASCO (middle panel), and the Wolf Sunspot Number (lower panel) averaged over 5 solar rotations, all for the time period 1995–2003. The horizontal bars in the upper panel show the average duration of ICMEs enlarged by a factor of 100, while the vertical bars indicate the effect of changing the number of events by one in each time bin.

increasing or reducing one event in each time bin, a way showing confidence levels. The occurrence rate of ICMEs does not strictly follow the variation of the sunspot number. One notable feature is the dip in the number of ICMEs between 1998 and 1999, with no corresponding reduction in the sunspot number. The two maxima in the top panel are generally matched by the two peaks in the bottom panel. These results are similar to those obtained by Cane and Richardson (2003). The horizontal bars indicate the average ICME duration in each bin enlarged by a factor of 100. Although the duration is generally longer during solar maximum, it does not closely trace the sunspot number. The variation of the ICME rate is generally similar to that of LASCO CMEs, except that the first ICME peak is higher than the second one, whereas the two peaks of the smoothed CME rate have the same height.

Fig. 9 displays the duration of ICMEs observed by WIND and ACE from 1995 to 2002 as a function of the bulk speed. Each ICME is represented by a dot with radial width proportional to the radius of the dot. The color bar shows the time when each ICME was observed to show the solar cycle variation of these parameters. Since the radial width of ICMEs is the product of the speed and the duration, the radial width increases with speed at a fixed duration or with duration at a fixed speed. The average speeds for individual ICMEs vary from 340 to 700 km s^{-1}, with a mean value of 458.6 km s^{-1}; the average duration lies between 6 and 86.4 h with a mean value of 30.4 h. The average size in the radial direction ranges from 0.07 to 1.19 AU and has a mean value of 0.34 AU. Note that most of the long, high-speed events, represented by big spots, were observed during solar maximum, in agreement with the radial width variation shown in Fig. 8.

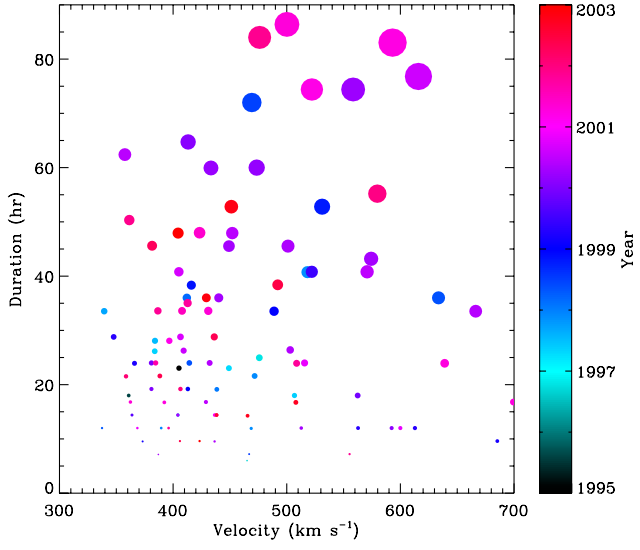

Fig. 9. Duration versus bulk speed for ICMEs at 1 AU. The radius of the circle for each ICME is proportional to its radial width. The color bar shows the time when each ICME was observed.

5. Conclusions

We used the signatures of helium abundance enhancement and temperature depression to identify ICMEs from in situ measurements of the solar wind by spacecraft with heliocentric distances ranging from 0.3 to 5.4 AU. We then investigated the propagation of ICMEs in the heliosphere in a statistical sense. The results are summarized as follows.

ICMEs expand as they move outward. Their radial width increases by a factor of 4 from 1 to 5 AU, proportional to $R^{0.92}$. The plasma density and magnetic field magnitude inside ICMEs decrease faster than those in the solar wind. The temperature, however, decreases more slowly in ICMEs than in the solar wind. The slower decrease of temperature implies considerable heating of the ejecta. The average bulk speed of ICMEs remains constant with distance, whereas the expansion speed decreases very slowly, suggestive of a quasi-equilibrium expansion. Comparison in the standard deviation of speed between ICMEs and the solar wind shows that about 77% of events observed at distances larger than 5.15 AU have speed variations smaller than the average solar wind value.

The ICME expansion is governed by a polytrope of $\gamma = 1.15$, which was determined empirically. The polytropic index was found to be independent of heliocentric distance and solar cycle. The electron-to-proton pressure ratio is about 3.25, showing that electrons dominate the contribution to the thermal pressure. The polytropic index is not changed by inclusion of the electron pressure nor the magnetic pressure. The polytropic index for ICME electrons, γ_e, is about 0.73, conflicting with the observed decrease in temperature. This discrepancy can be explained by non-Maxwellian distributions of electrons.

The occurrence rate of ICMEs at 1 AU roughly follows the solar cycle variation, except for a dip between 1998 and 1999 that is not present in the time profile of the sunspot number. The radial width of ICMEs also has a solar cycle dependence, with a mean value of 0.34 AU averaged over the whole solar cycle.

Acknowledgements

We are grateful to the ACE and Ulysses experimenters who have made their data available at NSSDC. We also acknowledge the use of the Helios data provided by R. Schwenn. One author (Y. Liu) thanks J.C. Kasper

for his help in analyzing the WIND data. The work was supported by NASA Grant NAG-10915 and by NSF Grants ATM-0203723 and ATM-0207775.

References

Borrini, G., Gosling, J.T., Bame, S.J., Feldman, W.C., 1982. Helium abundance enhancements in the solar wind. J . Geophys. Res. 87, 7370.

Bothmer, V., Schwenn, R., 1998. The structure and origin of magnetic clouds in the solar wind. Ann. Geophys. 16, 1.

Burlaga, L.F., 1988. Magnetic clouds and force-free fields with constant alpha. J. Geophys. Res. 93, 7217.

Burlaga, L.F., Ogilvie, K.W., 1970. Heating of the solar wind. Astrophys. J. 159, 670.

Burlaga, L.F., Ogilvie, K.W., 1973. Solar wind temperature and speed. J. Geophys. Res. 78, 2028.

Burlaga, L., Sittler, E., Mariani, F., Schwenn, R., 1981. Magnetic loop behind an interplanetary shock: Voyager, Helios and IMP 8 observations. J. Geophys. Res. 86, 6673.

Cane, H.V., Richardson, I.G., 2003. Interplanetary coronal mass ejections in the near-Earth solar wind during 1996–2002. J. Geophys. Res. 108 (10.1029/2002JA00981).

Cargill, P.J., Spicer, D.S., Zalesak, S.T., 1997. Magnetohydrodynamic simulations of Alfvénic pulse propagation in solar magnetic flux tubes: two-dimensional slab geometries. Astrophys. J. 488, 854.

Chen, J., 1996. Theory of prominence eruption and propagation: interplanetary consequences. J. Geophys. Res. 101, 27499.

Chen, J., Garren, D.A., 1993. Interplanetary magnetic clouds: topology and driving mechanism. Geophys. Res. Lett. 20, 2319.

Dungey, J.W., 1961. Interplanetary magnetic field and the auroral zones. Phys. Rev. Lett. 6, 47.

Gazis, P.R., Bames, A., Mihalov, J.D., Lazarus, A.J., 1994. Solar wind velocity and temperature in the outer heliosphere. J. Geophys. Res. 99, 6561.

Gibson, S.E., Low, B.C., 1998. A time dependent three-dimensional magnetohydrodynamic model of the coronal mass ejection. Astrophys. J. 493, 460.

Goldstein, R., Neugebauer, M., Clay, D., 1998. A statistical study of coronal mass ejection plasma flows. J. Geophys. Res. 103, 4761.

Gosling, J.T., Pizzo, V., Bame, S.J., 1973. Anomalously low proton temperatures in the solar wind following interplanetary shock waves: evidence for magnetic bottles? J. Geophys. Res. 78, 2001.

Gosling, J.T., Baker, D.N., Bame, S.J., Feldman, W.C., Zwickl, R.D., Smith, E.J., 1987. Bidirectional solar wind electron heat flux events. J. Geophys. Res. 92, 8519.

Hirshberg, J., Bame, S.J., Robbins, D.E., 1972. Solar flares and solar wind helium enrichments: July 1965–1967. Sol. Phys. 23, 467.

Kahler, S.W., Reames, D.V., 1991. Probing the magnetic topologies of magnetic clouds by means of solar energetic particles. J. Geophys. Res. 96, 9419.

Krall, J., Chen, J., Santoro, R., 2000. Drive mechanisms of erupting solar magnetic flux ropes. Astrophys. J. 539, 964.

Kumar, A., Rust, D.M., 1996. Interplanetary magnetic clouds, helicity conservation, and current-core flux ropes. J. Geophys. Res. 101, 15667.

Lepping, R.P., et al., 1995. The wind magnetic field investigation. Space Sci. Rev. 71, 207.

Lopez, R.E., Freeman, J.W., 1986. Solar wind proton temperature-velocity relationship. J. Geophys. Res. 91, 1701.

Montgomery, M.D., Asbridge, J.R., Bame, S.J., Feldman, W.C., 1974. Solar wind electron temperature depressions following some interplanetary shock waves: evidence for magnetic merging? J. Geophys. Res. 79, 3103.

Musmann, G., Neubauer, F.M., Maier, A., Lammers, E., 1975. Das Förstersonden-Magetfeldexperiment (E2). Raumfahrtforschung 19/5, 232.

Ogilvie, K.W., et al., 1995. A comprehensive plasma instrument for the wind spacecraft. Space Sci. Rev. 71, 41.

Osherovich, V.A., Farrugia, C.J., Burlaga, L.F., 1993a. Nonlinear evolution of magnetic flux ropes: 1. The low beta limit. J. Geophys. Res. 98, 1325.

Osherovich, V.A., Farrugia, C.J., Burlaga, L.F., 1993b. Dynamics of aging magnetic clouds. Adv. Space Res. 13, 57.

Osherovich, V.A., Farrugia, C.J., Burlaga, L.F., Lepping, R.P., Fainberg, J., Stone, R.G., 1993c. Polytropic relationship in interplanetary magnetic clouds. J. Geophys. Res. 98, 15331.

Palmer, I.D., Allum, F.R., Singer, S., 1978. Bidirectional anisotropies in solar cosmic ray events: evidence for magnetic bottles. J. Geophys. Res. 83, 75.

Paularena, K.I., Wang, C., von Steiger, R., Heber, B., 2001. An ICME observed by Voyager 2 at 58 AU and by Ulysses at 5 AU. Geophys. Res. Lett. 28, 2755.

Phillips, J.L., et al., 1995. Ulysses solar wind plasma observations at high southernly latitudes. Science 268, 1030.

Rao, U.R., McCracken, K.G., Bukata, R.P., 1967. Cosmic ray propagation processes, 2, The energetic storm particle event. J. Geophys. Res. 72, 4325.

Richardson, I.G., Cane, H.V., 1993. Signatures of shock drivers in the solar wind and their dependence on the solar source location. J. Geophys. Res. 98, 15295.

Richardson, I.G., Cane, H.V., 1995. Regions of abnormally low proton temperature in the solar wind (1965–1991) and their association with ejecta. J. Geophys. Res. 100, 23397.

Richardson, I.G., Reames, D.V., 1993. Bidirectional ~ 1 MeV ion intervals in 1973–1991 observed by the Goddard Space Flight Center instruments on IMP 8 and ISEE 3/ICE. Astrophy. J. 85 (Suppl. Ser.), 411.

Richardson, J.D., Smith, C.W., 2003. The radial temperature profile of the solar wind. Geophys. Res. Lett. 30 10.1029/2002GL016551.

Richardson, J.D., Paularena, K.I., Lazarus, A.J., Belcher, J.W., 1995. Radial evolution of the solar wind from IMP 8 to Voyager 2. Geophys. Res. Lett. 22, 325.

Richardson, J.D., Paularena, K.I., Wang, C., Burlaga, L.F., 2002. The life of a CME and the development of a MIR: from the Sun to 58 AU. J. Geophys. Res. 107 10.1029/2001JA000175.

Richardson, J.D., Wang, C., Burlaga, L.F., 2004. The solar wind in the outer heliosphere. Adv. Space Res. 34, 150.

Rosenbauer, H., Schwenn, R., Miggenrieder, H., Meyer, B., Grünwaldt, H., Mühlhäuser, K.-H., Pelkofer, H., Wolfe, J.H., 1981. Die Instrumente des plasmaexperimentes auf den HELIOS-Sonnensonden, Luft-und Raumfahrt, Weltraumforschung/Weltraumtechnologie. BMFT-FB, W81-015.

Schwenn, R., Rosenbauer, H., Miggenrieder, H., 1975. Das Plasmaexperiment auf HELIOS (E1). Raumfahrtforschung 19/5, 226.

Scudder, J.D., 1992. On the causes of temperature change in inhomogeneous low-density astrophysical plasmas. Astrophys. J. 398, 299.

Sittler Jr., E.C., Burlaga, L.F., 1998. Electron temperatures within magnetic clouds between 2 and 4 AU: Voyager 2 observations. J. Geophys. Res. 103, 17447.

Sittler Jr., E.C., Scudder, J.D., 1980. An empirical polytrope law for solar wind thermal electrons between 0.45 and 4.76 AU: Voyager 2 and Mariner 10. J.Geophys. Res. 85, 5131.

Stone, E.C., Frandsen, A.M., Mewaldt, R.A., Christian, E.R., Margolies, D., Ormes, J.F., Snow, F., 1998. The Advanced Composition Explorer. Space Sci. Rev. 86, 1.

Suess, S.T., 1988. Magnetic clouds and the pinch effect. J. Geophys. Res. 93, 5437.

Temnyi, V.V., Vaisberg, O.L., 1979. A dumbbell distribution of epithermal electrons in the solar wind based on observations on the Prognoz 7 satellite. Cosmic Res. 17, 476.

Totten, T.L., Freeman, J.W., Arya, S., 1995. An empirical determination of the polytropic index for the free-streaming solar wind using Helios 1 data. J. Geophys. Res. 100, 13.

Vandas, M., Fischer, S., 1996. Parametric study of loop-like magnetic cloud propagation. J. Geophys. Res. 101, 15645.

Vandas, M., Fischer, S., Pelant, P., Geranios, A., 1993a. Spheroidal models of magnetic clouds and their comparison with spacecraft measurements. J. Geophys. Res. 98, 11467.

Vandas, M., Fischer, S., Pelant, P., Geranios, A., 1993b. Evidence for spheroidal structure of magnetic clouds. J. Geophys. Res. 98, 21061.

Wenzel, K.P., Marsden, R.G., Page, D.E., Smith, E.J., 1989. ULYSSES—the first high-latitude heliospheric mission. Adv. Space Res. 9, 25.